



Figures and figure supplements

A feedback mechanism converts individual cell features into a supracellular ECM structure in *Drosophila* trachea

Arzu Öztürk-Çolak et al

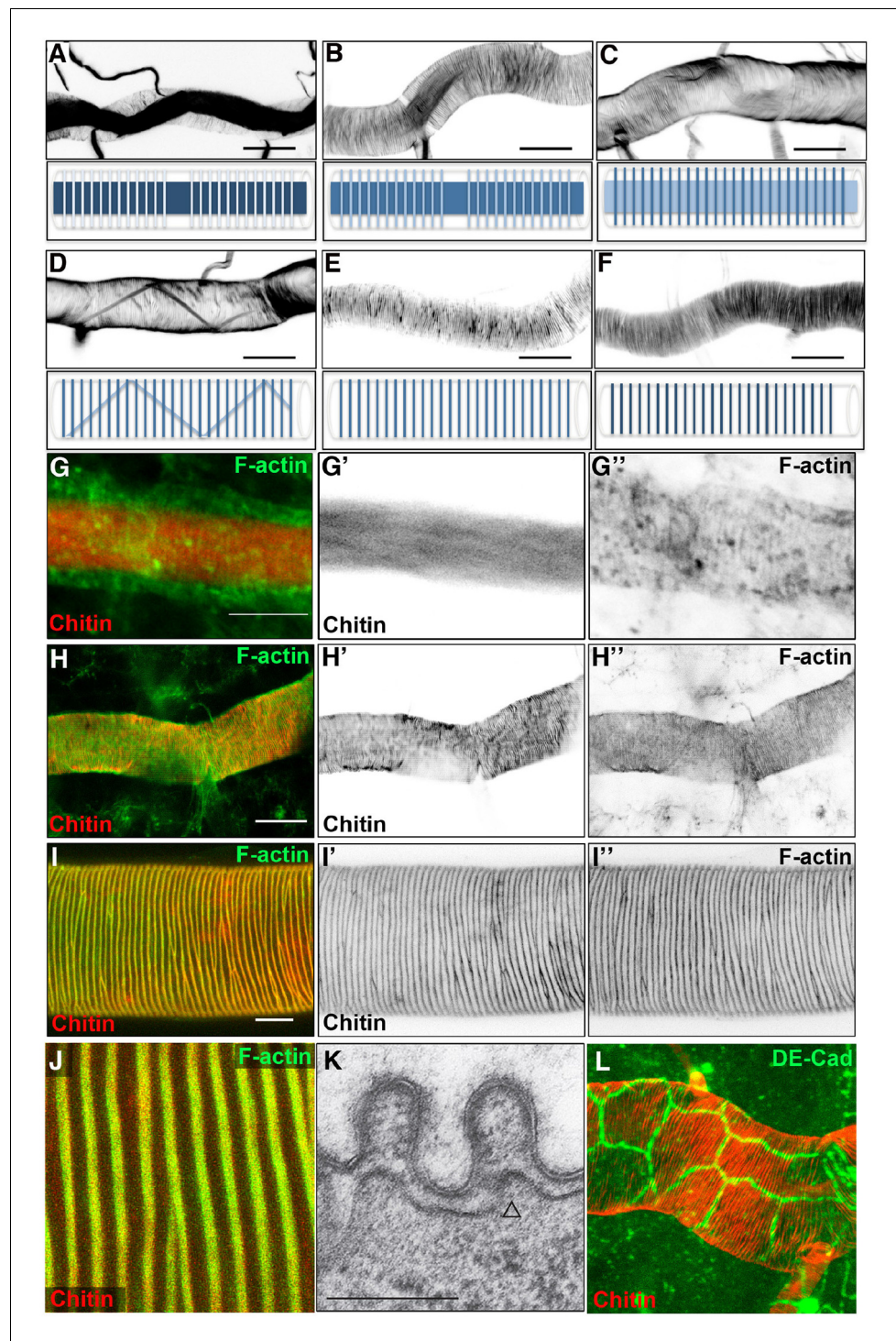


Figure 1. Dynamics of taenidial fold and actin ring formation. (A–F) Dorsal Trunk detail of wild-type embryos stained with fluostain to label the chitin structures. Maximum projections of confocal Z sections showing the dynamics of intraluminal chitin filament and taenidial folds during late stages of embryonic development. Chitin structures are schematically represented under each image. Chitin filament: at late stage 16, intraluminal chitin filament is thick and dense (A); as the embryo develops, it becomes less and less dense (B, C) until it turns into a thin chitin fibre that runs in zigzags along the tube diameter (D); in the last steps of embryogenesis, the intraluminal chitin filament is completely cleared from the lumen (E, F). Taenidial folds: at late stage 16, taenidial folds are newly formed and thin (A); as the taenidial folds become thicker, it is apparent that the taenidial folds at fusion points are not formed yet (B); later, the taenidial folds at fusion points are also formed which generates a

Figure 1 continued on next page

Figure 1 continued

continuous taenidial structure along the tube (C); in the final steps, as the intraluminal chitin filament is cleared from the lumen, the taenidial folds reach their the most mature form (D–F). Scale bars = 10 μm . (G–J) wild-type embryonic (G–H) and 3rd instar larval (I–J) trachea stained with fluostain (red) and phalloidin (green) showing taenidial folds and F-actin bundles together (G, H, I, J) or separately (G', G'', H', H'' and I', I''). F-actin organisation in structures perpendicular to the main tube axis occurs at stage 16 prior to taenidial fold appearance (G). When taenidia become apparent (H), they are positioned over the actin bundles and this co-localisation continues throughout larval stages (I, J). Scale bars = 10 μm . (K) TEM detail of wild-type DT taenidia, the open triangle points to actin filament cross-sections (diameter around 7 nm). Scale bar 250 nm. (L) Detail of DT showing apical cell borders (labelled by anti-DE-Cad in green) and how taenidia (labelled by fluostain in red) span continuously beyond cell-cell borders from one cell to the other.

DOI: [10.7554/eLife.09373.003](https://doi.org/10.7554/eLife.09373.003)

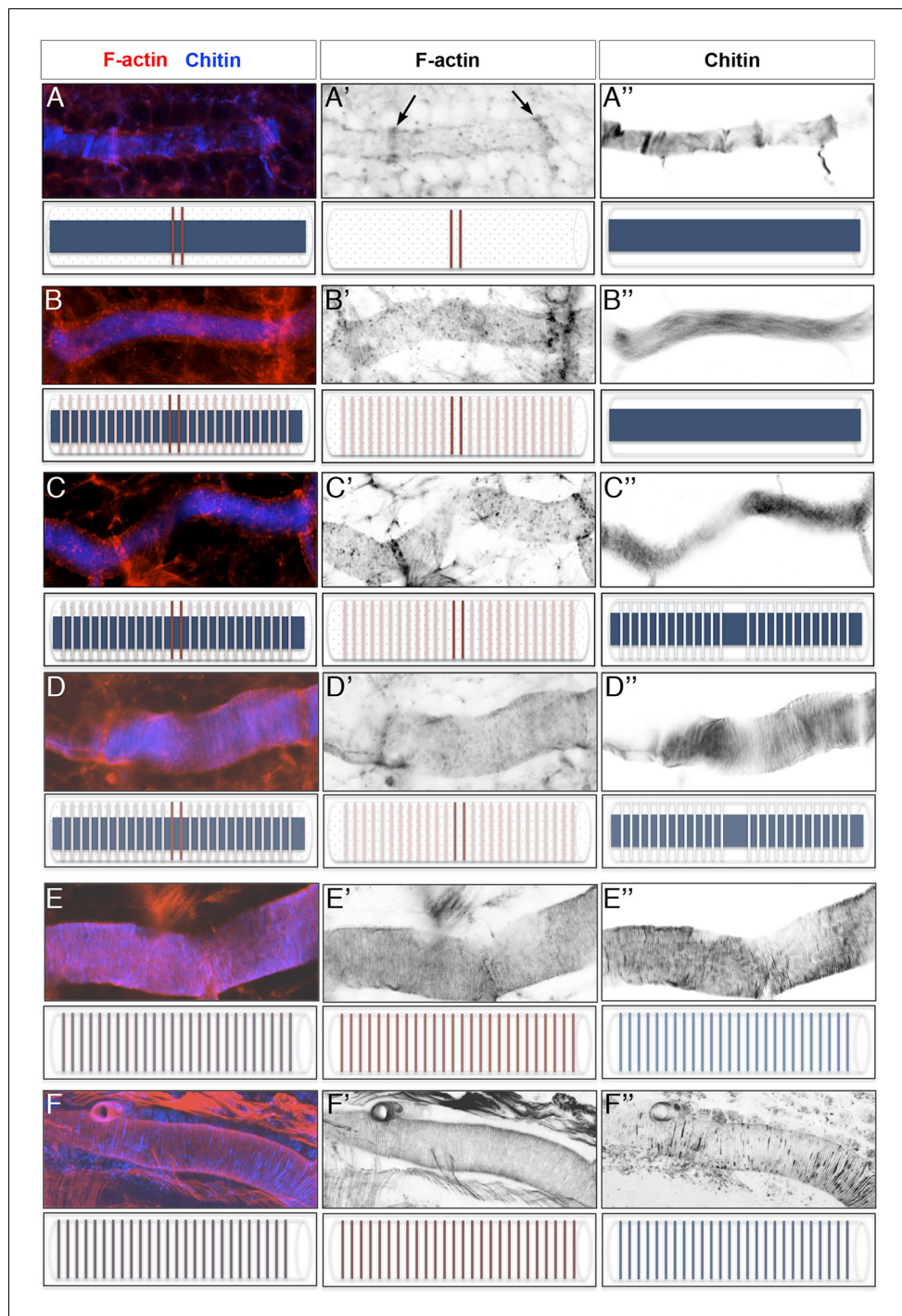


Figure 1—figure supplement 1. Time course of actin ring and taenial fold formation. (A–F) Projections of confocal sections of wild-type DTs from early stage 16 to stage 17. F-actin is detected by phalloidin (red) and Chitin by fluostain (blue). The F-actin (red) and chitin (blue) structures are schematically represented under each image. First F-actin bundles are formed at the fusion points during the fusion process of the DT (A', arrows). These bundles are formed as a result of highly orchestrated cell shape changes during fusion events. At mid-stage 16, F-actin rings become visible along the DT while the taenial folds are not fully formed yet and hence not labelled with fluostain (B). Then, very thin taenial folds become visible (C). At first, they are not formed at fusion points (D). Later, taenial folds at fusion points are also formed, thus generating a continuous taenial structure along the tube (E). Finally, the taenial folds and F-actin bundles reach their most mature form as the trachea start to fill
Figure 1—figure supplement 1 continued on next page

Figure 1—figure supplement 1 continued

with air (F). Both stainings are shown in the merge images (A-F). The fluostain (A'-F') and phalloidin (A''-F'') stainings are shown separately.

DOI: [10.7554/eLife.09373.004](https://doi.org/10.7554/eLife.09373.004)

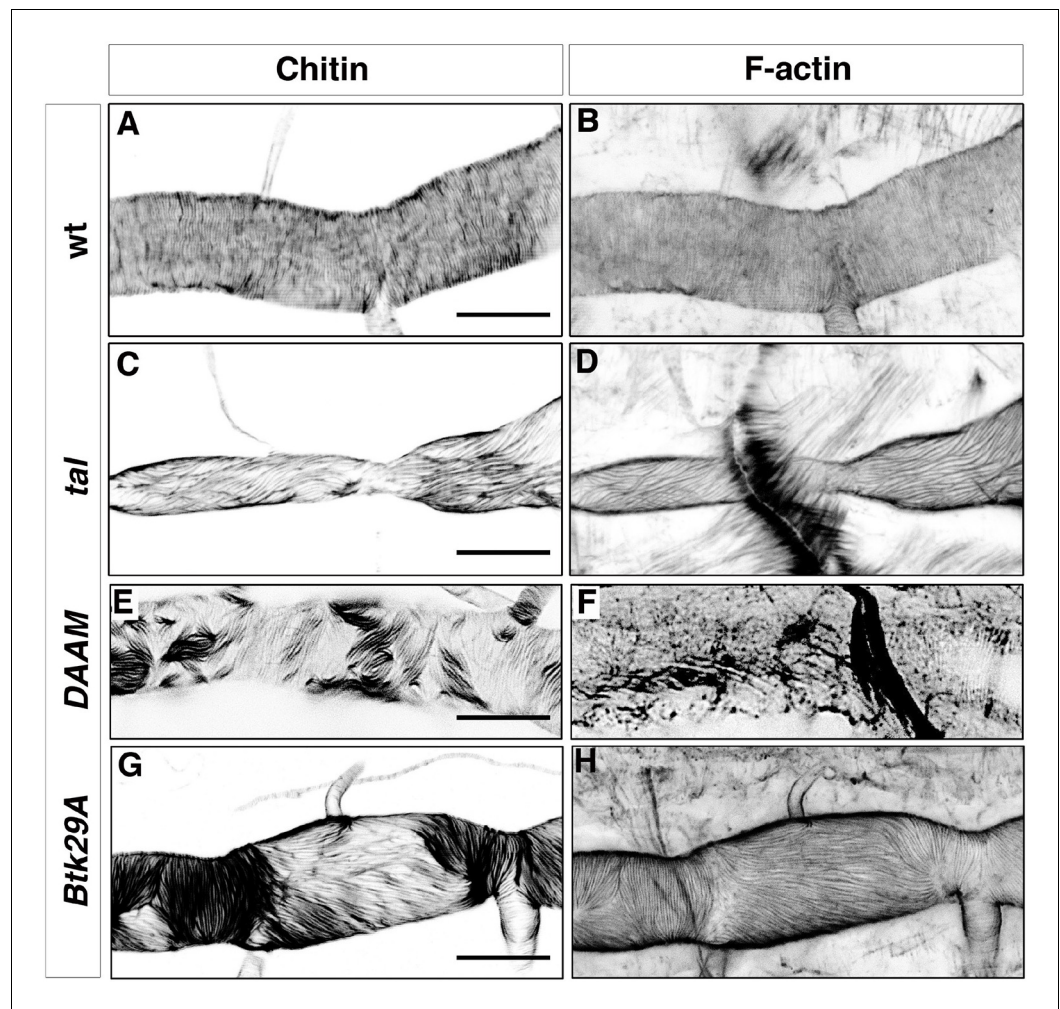


Figure 2. Taenial folds and F-actin rings in *tal/pri*, *DAAM*, and *Btk29A* mutants. Wild-type (A, B), *tal/pri* (C-D), *DAAM* (E-F), and *Btk29A* (G-H) mutant embryos stained with fluostain (A, C, E, G) to label taenial folds and phalloidin (B, D, F, H) to label F-actin bundles. Both taenial folds and F-actin bundles run perpendicular to the tube axis in wild-type embryos (A, B) while in most of the *pri* mutants they are parallel to the tube axis (C, D). In *DAAM* (E-F) and *Btk29A* (G-H) mutant embryos, taenial folds and actin bundles are hardly detected and when so they appear mis-oriented, running both parallel and perpendicular to the tube axis. In all panels anterior is to the left and scale bars =10 μ m.

DOI: [10.7554/eLife.09373.005](https://doi.org/10.7554/eLife.09373.005)

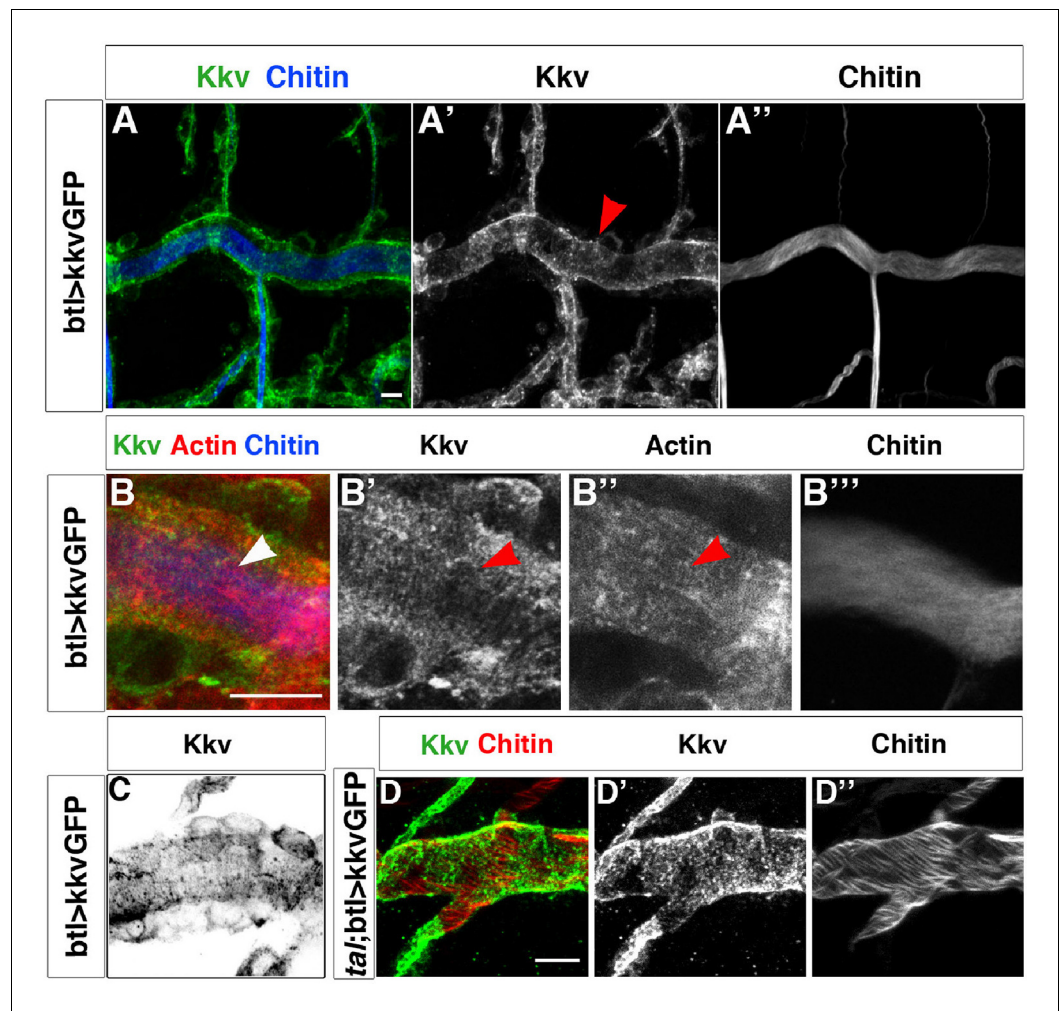


Figure 3. Kkv co-localises with F-actin rings during tracheal maturation. (A) Detail of stage 16 wild-type embryos expressing a *kkvGFP* transgene in tracheal cells and stained with fluostain to reveal the chitin filament; Kkv is detected in rings that resemble the F-actin rings (arrowhead in A'). (B) DT zoomed detail of stage 16 wild-type embryos expressing a *kkvGFP* transgene in tracheal cells and stained with fluostain and phalloidin to reveal the chitin filament and the F-actin rings (arrowheads). (C) Detail of a stage 17 embryo expressing *kkvGFP* in tracheal cells, showing the localisation of Kkv in rings throughout the length of the tube. (D) Detail of stage 17 *tal/pri* embryos expressing a *kkvGFP* transgene and stained with fluostain to reveal the chitin aECM; in *tal/pri* mutants, Kkv is detected in a punctate pattern throughout stages 16–17 and not in lines or bundles, in contrast to wild-type embryos. In all panels anterior is to the left and scale bars = 10 μ m.

DOI: [10.7554/eLife.09373.006](https://doi.org/10.7554/eLife.09373.006)

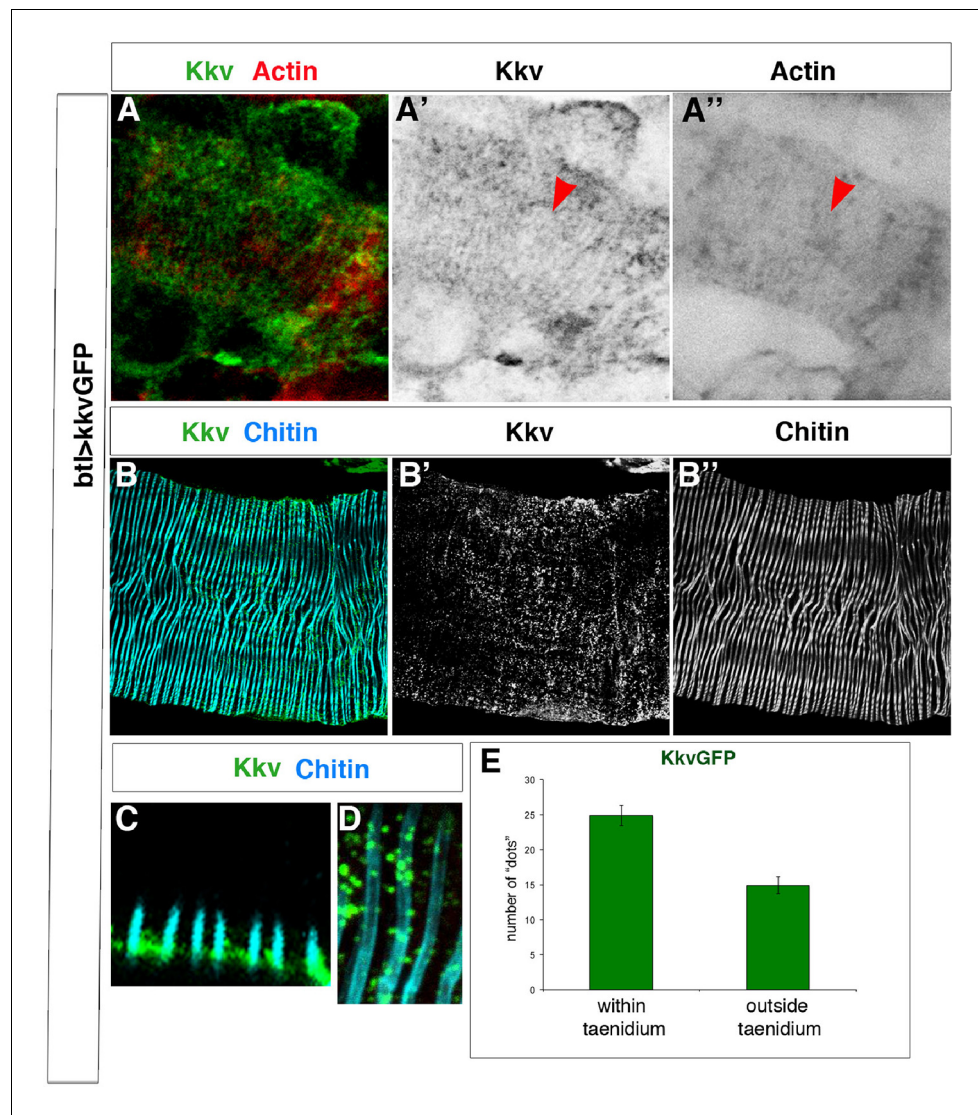


Figure 3—figure supplement 1. Kkv co-localises with F-actin and chitin rings at embryonic and larval stages. (A) Detail of stage 16 wild-type embryos expressing a *kvvGFP* transgene in tracheal cells and stained with phalloidin to reveal the F-actin rings; Kkv is detected in rings that resemble the F-actin rings (arrowhead in A'). (B) DT zoomed detail of an L3 larva expressing a *kvvGFP* transgene in tracheal cells and stained with anti-GFP antibody to detect KkvGFP localisation and fluostain to reveal the chitin filament. (C) Zoomed detail of the apical membrane of the tracheal cells of an L3 larva expressing a KkvGFP showing how the larger KkvGFP units overlap with the taenidia. (D) Zoomed detail of the DT of an L3 larva expressing a KkvGFP showing how the larger KkvGFP units overlap with the taenidia. (E) Quantification of the number of KkvGFP dots that overlap within the taenidium (mean of 24.8 ± 1.4 , $n = 24$) in comparison to the dots localised outside the taenidium (mean of 14.8 ± 1.2 , $n = 24$). Error bars represent \pm SEM and p-value is $3.1E-6$ by two-tailed unpaired Student's t-test.

DOI: [10.7554/eLife.09373.007](https://doi.org/10.7554/eLife.09373.007)

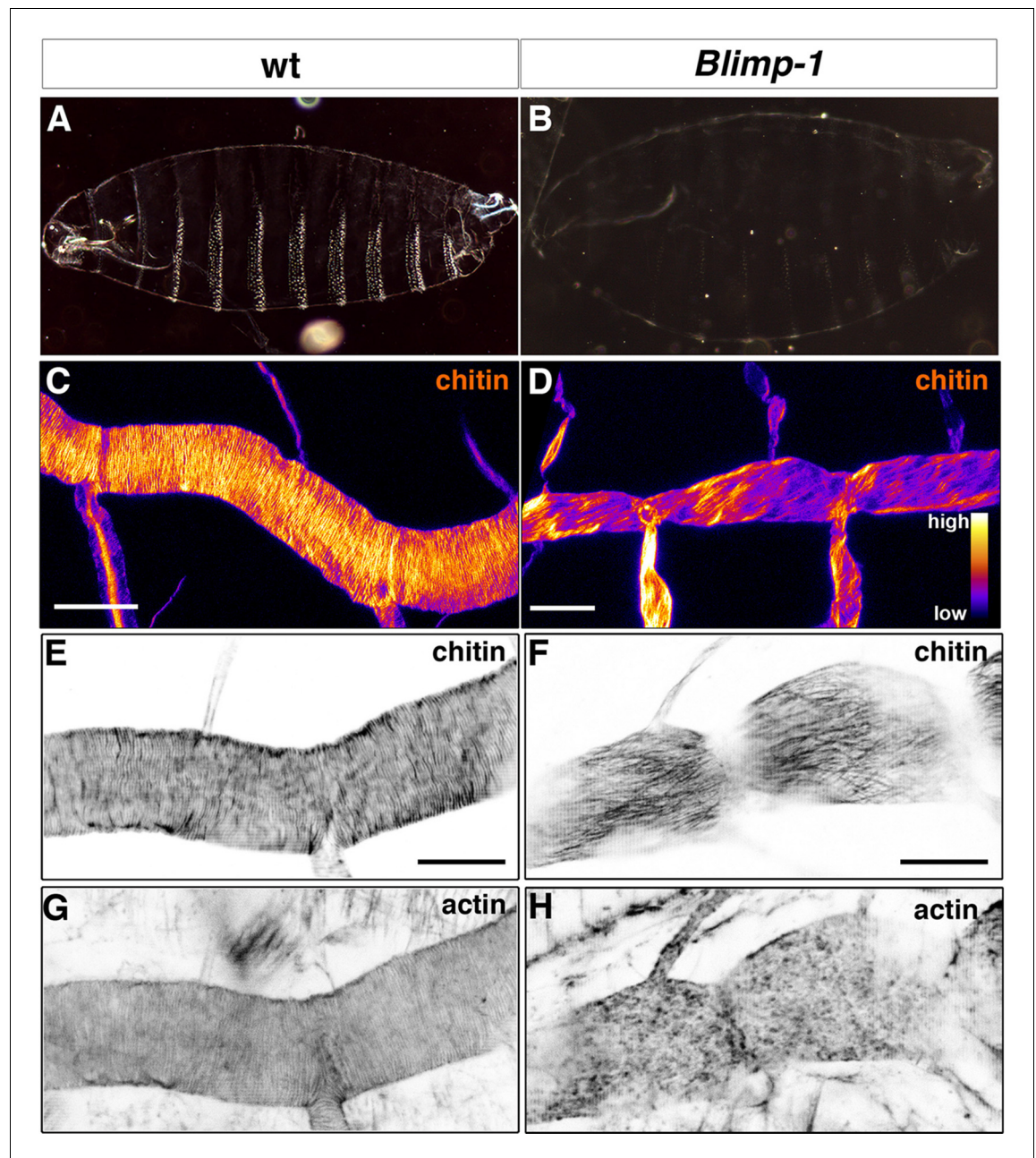


Figure 4. Taenial folds, F-actin bundles, and chitin levels in *Blimp-1* mutant embryos. (A-B) Cuticle preparations of wild-type (A) and *Blimp-1* (B) embryos visualised under dark field. In the *Blimp-1* mutant embryo, the cuticle and the denticle belts, chitin structures at the epidermis, are faint when compared to wild-type preparation. (C-D) Stage 17 *Blimp-1* heterozygous (control, C) and *Blimp-1* homozygous mutant (D) embryos stained with fluostain to label chitin structures. After acquisition in the same conditions, the images are converted into colour-coded LUTs in which different levels of fluorescent signals are matched with different colours. The colour code is shown on the lower right hand of panel D. While in the control DT mostly red and yellow stains are observed, in the *Blimp-1* mutant DT there are mostly purple and red stains, indicating that the fluorescent signal level of fluostain is lower in the *Blimp-1* mutant DT. Scale bars = 10 μ m. (E-H) Wild-type (E, G) and *Blimp-1* mutant embryos (F, H) stained with fluostain (E, F) to label taenial folds and phalloidin (G, H) to label F-actin bundles. Both the taenial folds and F-actin bundles run perpendicular to the tube axis in wild-type embryos (E, G) while in most of the *Blimp-1* mutants F-actin bundles fail to form (H) and taenial folds run parallel to the tube axis (F). The images are single stacks of confocal sections. Scale bars = 10 μ m.

DOI: [10.7554/eLife.09373.008](https://doi.org/10.7554/eLife.09373.008)

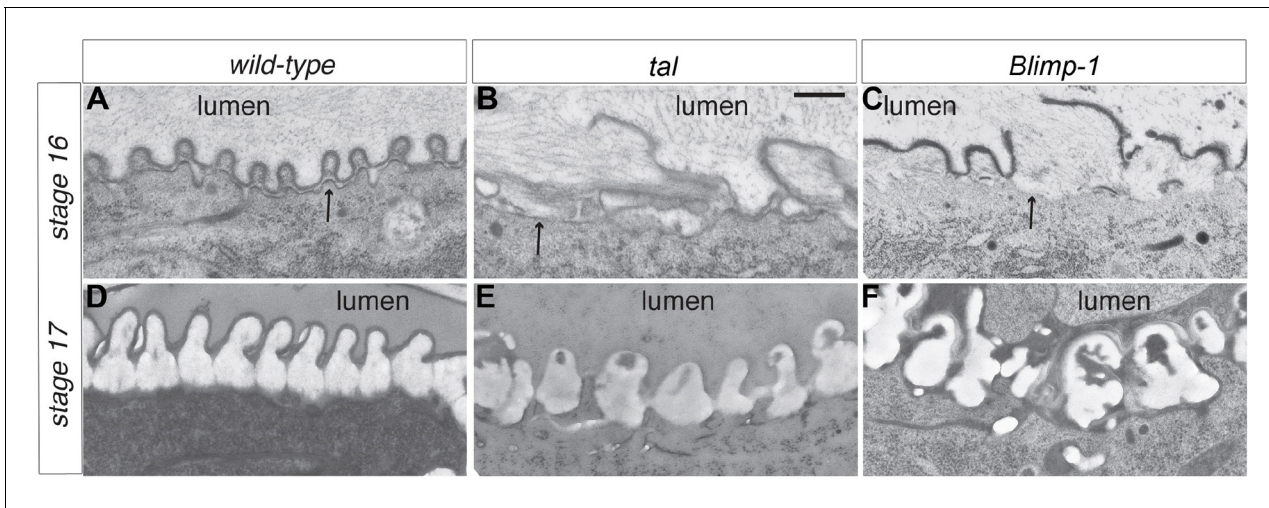


Figure 5. Taenidial structure in *tal/pri* and *Blimp-1* embryos. (A-F) Electron-micrographs of longitudinal sections of the dorsal trunk in wild-type, *tal/pri* and *Blimp-1* embryos. (A) In wild-type stage 16 embryos, regular protrusions of the apical plasma membrane (arrow) of dorsal trunk cells produce the extracellular taenidial cuticle that mainly consists of the inner procuticle (pro) and the outer envelope (env). (B,C) In *tal/pri* and *Blimp-1* mutant stage 16 embryos, protrusions of the apical plasma membrane are irregular with occasionally extended flat regions. The taenidial cuticle follows these irregularities, and the envelope is discontinuous. (D) In wild-type stage 17 embryos, prior to hatching, the fully differentiated taenidial cuticle is characterised by folds of nearly equal breadth. (E,F) In contrast, in *tal/pri* and *Blimp-1* mutant stage 17 embryos the breadth of the differentiated taenidial folds is highly variable. Scale bar 500 nm applies to all electron-micrographs.

DOI: [10.7554/eLife.09373.011](https://doi.org/10.7554/eLife.09373.011)

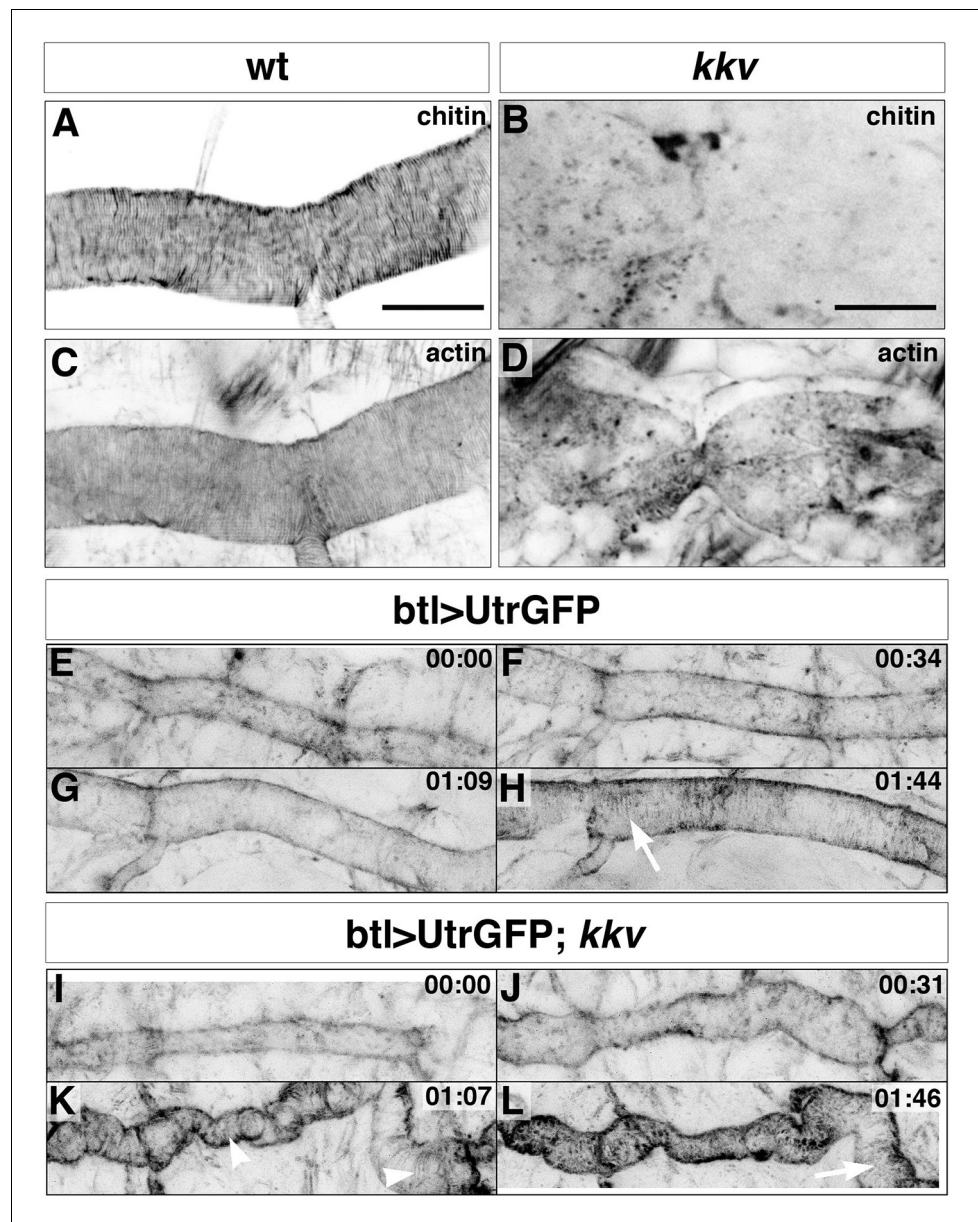


Figure 6. Taenidial folds and F-actin bundles in *kkv* mutant embryos. (A-D) *Wild-type* (A, C) and *kkv* mutant (B, D) mutant embryos stained with fluostain to label taenidial folds (A, B) and phalloidin to label F-actin bundles (C, D). The taenidial folds and F-actin bundles run perpendicular to the tube axis in the *wild-type* embryo (A, C) while in *kkv* mutant embryos taenidial folds are absent and F-actin bundles fail to form (B-D). The images are single stacks of confocal sections. Scale bars = 10 μ m. (E-L) Time-lapse images of *wild-type* (E-H) and *kkv* mutant (I-L) embryos carrying *btI>GAL4UASUtrGFP* to visualise actin in live embryos. In the *wild-type* embryo, F-actin bundles (arrow) become visible at the end of time-lapse imaging (H) while in the *kkv* mutant F-actin bundles form transiently (K, arrowhead) and then disappear (L, arrow).

DOI: [10.7554/eLife.09373.012](https://doi.org/10.7554/eLife.09373.012)

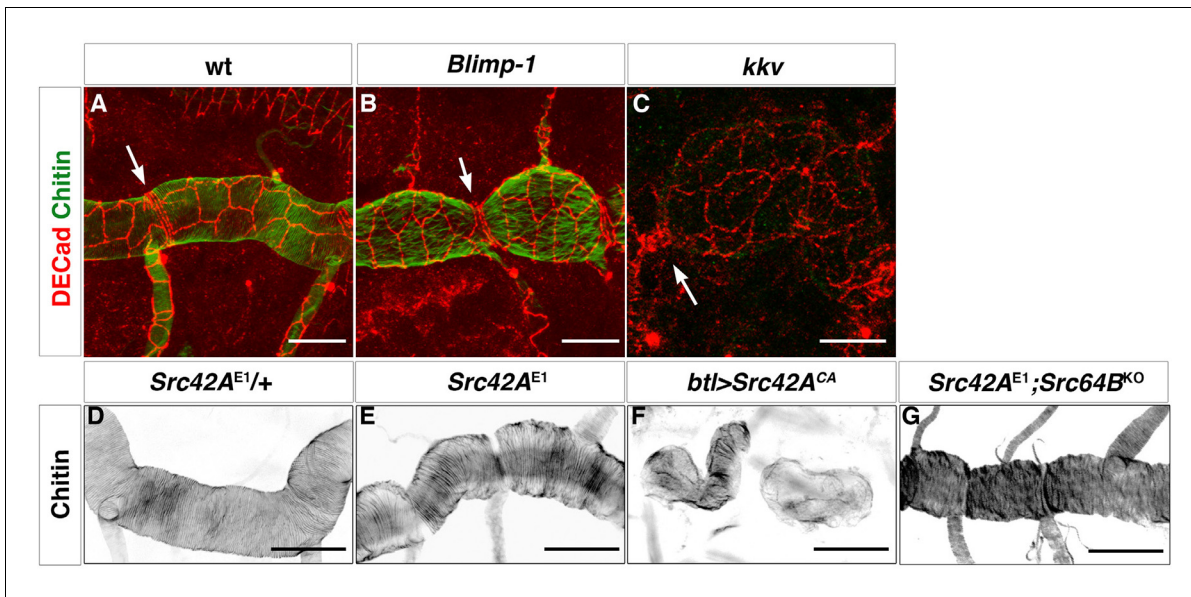


Figure 7. Apical cell shape in the *Blimp-1* and *kvv* mutant embryos. *Wild-type* (A), *Blimp-1* mutant (B) and *kvv* mutant (C) embryos stained with anti-DE-cad (red) to label the cell surface and fluostain (green) to label taenial folds. In the *Blimp-1* mutant embryo, apical cell shape is elongated perpendicular to the tube axis (B), whereas it is mostly parallel to the tube axis in the *wild-type* embryo (A). In the *kvv* mutant embryo, apical cell shape resembles more the *Blimp-1* phenotype (C). The distinct apical cell shape of the fusion cells (A, arrow) does not seem to be affected by the loss of function of *Blimp-1* (B, arrow) but is affected by the absence of *kvv* (C, arrow). The images are projections of confocal sections. Scale bars = 10 μm . (D-F) *Wild-type* (D) and *Src42A* mutant (E) embryos and the effect of constitutively activated *Src42A* on tracheal cells (F) of embryos stained with fluostain to label taenial folds. The taenial folds run perpendicular to the tube axis in *wild-type* (D), *Src42A* mutant (E) and *Src42A;Src64B* double mutant (G) embryos, whereas they are not properly formed in overexpression of *Src42A*^{CA} embryos (F). The images are projections of confocal sections. Scale bars = 10 μm .

DOI: [10.7554/eLife.09373.015](https://doi.org/10.7554/eLife.09373.015)

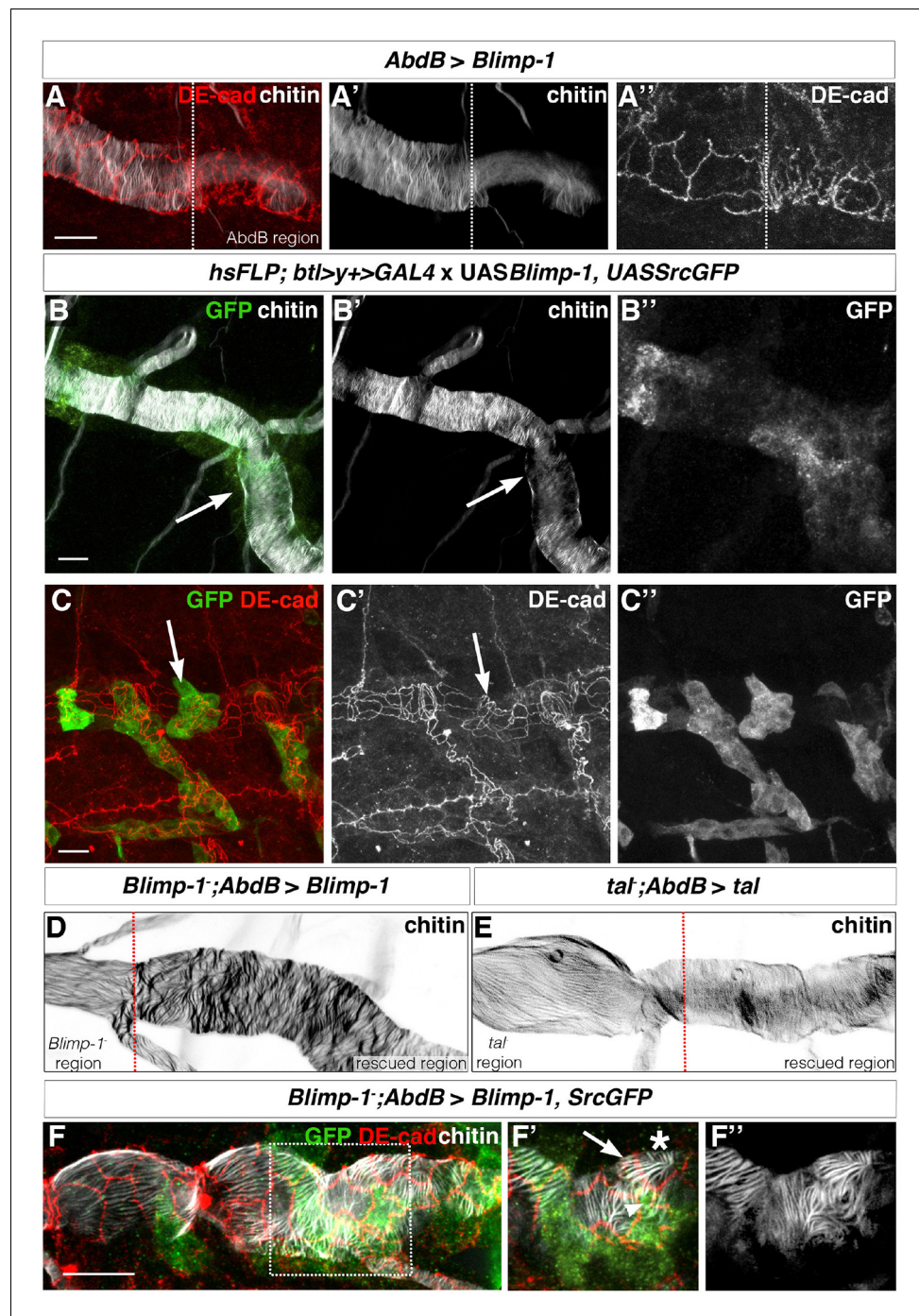


Figure 8. The orientation of taenial folds is not regulated autonomously. (A) *AbdB*GAL4-driven *UASBlimp-1* expression in a stage 17 wild-type embryo that is stained with fluostain to label taenial folds (A, A') and DE-cad to label adherens junctions (A, A'). In the region where *Blimp-1* is overexpressed, chitin is reduced and the apical surfaces of cells are altered. (B) An embryo with flip-out clones of overexpression of *Blimp-1* stained with fluostain (grey) to label taenial folds and anti-GFP (green) to detect expression of *UASSrcGFP* construct (and hence the clones). Note that the taenial folds that are formed within the clones (arrow) are thinner than neighbouring taenial folds formed by the cells outside the clones. The co-stainings are shown in the merge image (B). The chitin and anti-GFP stainings are shown separately (B', B''). (C) Embryos with flip-out clones of overexpression of *Blimp-1* stained with anti-DE-cad (red) to label the apical surface of the cells and anti-GFP (green) to detect expression of *UASSrcGFP* construct (hence the clones). Note that the shape of the apical surface of the cells in the clones (arrow) is altered when compared to the cells outside the clones. The co-stainings are shown in the merge image (C). (D) Embryo with flip-out clones of overexpression of *Blimp-1* stained with fluostain (grey) to label taenial folds and anti-GFP (green) to detect expression of *UASSrcGFP* construct (and hence the clones). Note that the taenial folds that are formed within the clones (arrow) are thinner than neighbouring taenial folds formed by the cells outside the clones. The co-stainings are shown in the merge image (D). (E) Embryo with flip-out clones of overexpression of *tal* stained with fluostain (grey) to label taenial folds and anti-GFP (green) to detect expression of *UASSrcGFP* construct (and hence the clones). Note that the taenial folds that are formed within the clones (arrow) are thicker than neighbouring taenial folds formed by the cells outside the clones. The co-stainings are shown in the merge image (E). (F) Embryo with flip-out clones of overexpression of *Blimp-1* stained with fluostain (grey) to label taenial folds and anti-GFP (green) to detect expression of *UASSrcGFP* construct (and hence the clones). Note that the taenial folds that are formed within the clones (arrow) are thinner than neighbouring taenial folds formed by the cells outside the clones. The co-stainings are shown in the merge image (F). (F') and (F'') show the chitin and anti-GFP stainings separately. Scale bars are shown in the bottom left of each panel.

Figure 8 continued on next page

Figure 8 continued

image (C). The anti-DE-cad and anti-GFP stainings are shown separately (C', C''). (D, E) *Blimp-1* mutant (D) and *tal/pri* mutant (E) embryos, carrying *AbdB-GAL4UASBlimp-1* (D) and *AbdBGAL4UASpri* (E) constructs, respectively, stained with fluostain to label taenidial folds (D, E). The orientation of taenidial folds that run parallel to the tube axis in *Blimp-1* and *tal/pri* mutant regions are rescued at the posterior part of the embryos, the rescued regions. The red dotted line separates the mutant from the rescued region, according to expression of GFP in the AbdB domain. (F) *Blimp-1* mutant embryo, carrying *UASBlimp-1* and *AbdBGAL4* constructs, stained with fluostain (grey) to label taenidial folds, GFP to show the AbdB domain and anti-DE-cad (red) to label apical surface of the cells. The *UASBlimp-1* construct is in a chromosome also carrying the *UASSrcGFP* construct and thus the anti-GFP (green) marks the area of *UASBlimp-1* expression. F' is a magnification of the rectangular region marked in F. The taenidial folds in the cell marked with an arrow (F') run parallel to the tube axis and are not 'rescued'. In contrast, the taenidial folds in the cell marked with an arrowhead (F') run perpendicular to the tube axis, because this cell carries the *UASBlimp-1* construct and hence it is 'rescued'. The cell marked with an asterisk has 'intermediate' taenidia displaying parallel and perpendicular orientation, dependent on the neighbouring cells. The triple-stainings are shown in the merge images (F, F'). The fluostain staining is shown separately (F'') to better assess the taenidial fold orientation. Scale bars 10 μm .

DOI: [10.7554/eLife.09373.016](https://doi.org/10.7554/eLife.09373.016)

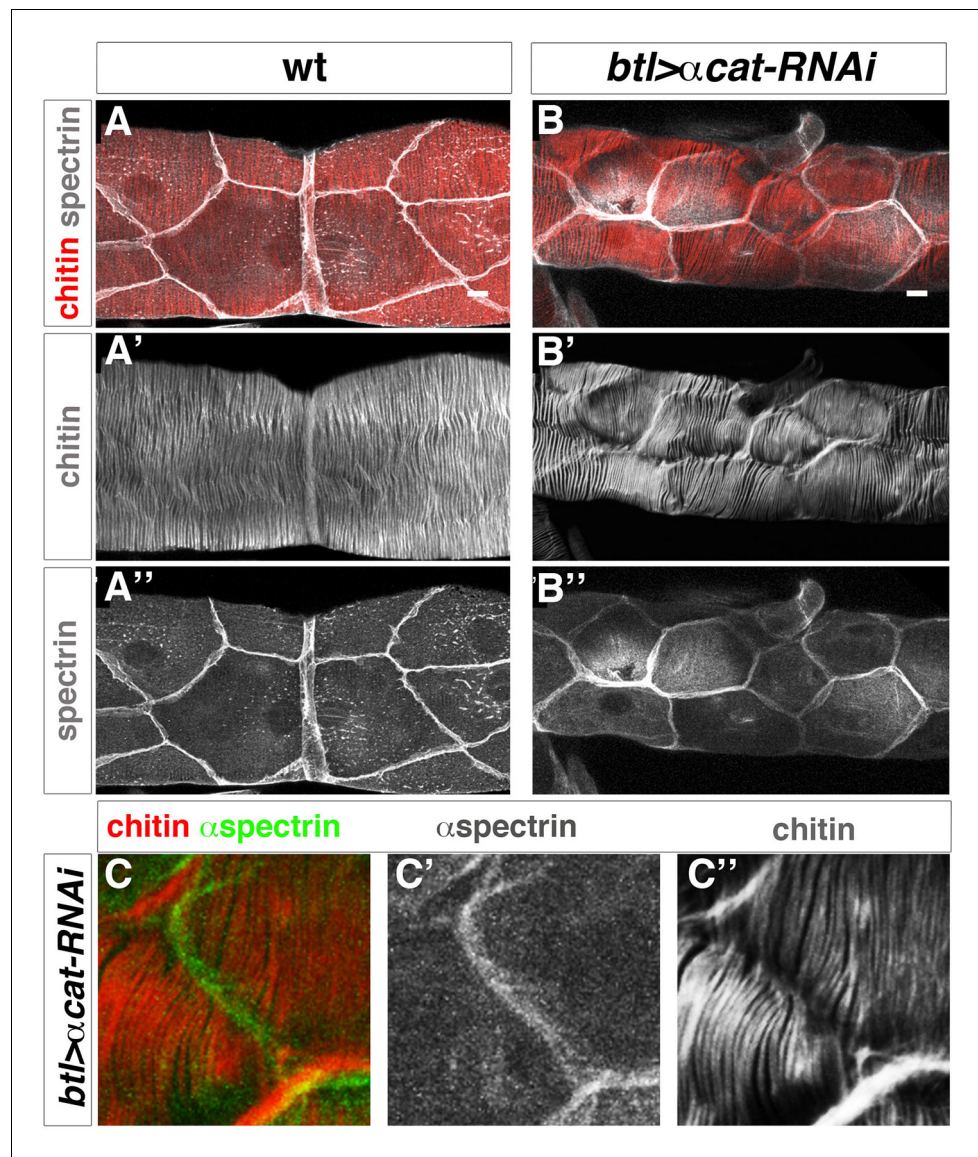


Figure 9. Taenidial folds in tracheal tubes with impaired cellular junctions. (A, B, C) Wild-type 3rd instar larval tracheas, carrying either no constructs (A) or *btl*-GAL4 and α -*cat*-RNAi constructs (B, C) stained with fluostain (red or grey) to label taenidial folds and anti-Spec (grey in A, B and C' and green in C) to label apical cell boundaries. The continuous taenidial folds in the wild-type larval trachea (A) become discontinuous at the apical cell boundaries upon down regulation of cellular junction components (B, C). The co-stainings are shown in the merge images (A, B and C). The fluostain (A', B', C') and anti-Spec (A'', B'' and C') stainings are shown separately. Scale bars 10 μ m.

DOI: [10.7554/eLife.09373.017](https://doi.org/10.7554/eLife.09373.017)

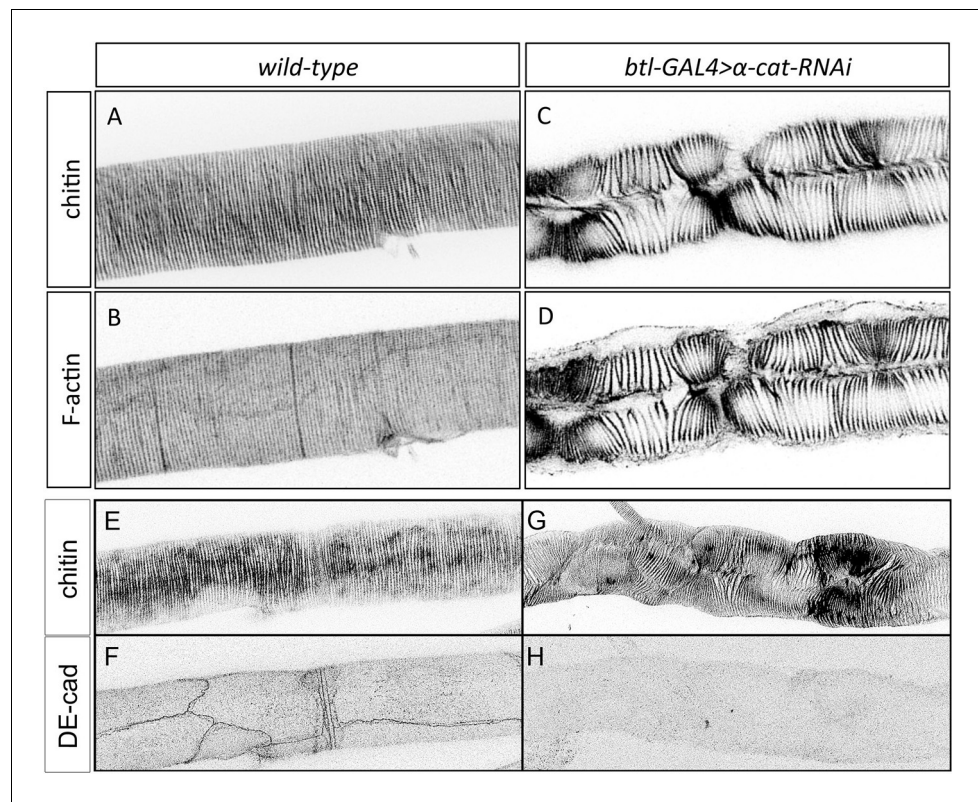


Figure 9—figure supplement 1. Taenidial folds in tracheal tubes with impaired cellular junctions. (A-D) Wild-type 3rd instar larval tracheal DT carrying either no constructs (A, B) or *btl-GAL4* and *α-cat-RNAi* constructs (C, D) stained with fluostain (A, C) to label taenidial folds and phalloidin (B, D) to label F-actin bundles. The continuous taenidial folds and F-actin bundles in the wild-type larval trachea (A, B) are disrupted upon down-regulation of cellular junction components (C, D). Images are single stacks of confocal sections. (E-H) *btlGAL4UASα-cat-RNAi*, 3rd instar larval tracheal DT stained with fluostain (E, G) and anti-DE-Cad (F,H) to detect the AJs. In embryos where *α-Cat* has been downregulated, DE-Cad is not detected (n = 17 larvae).

DOI: [10.7554/eLife.09373.018](https://doi.org/10.7554/eLife.09373.018)

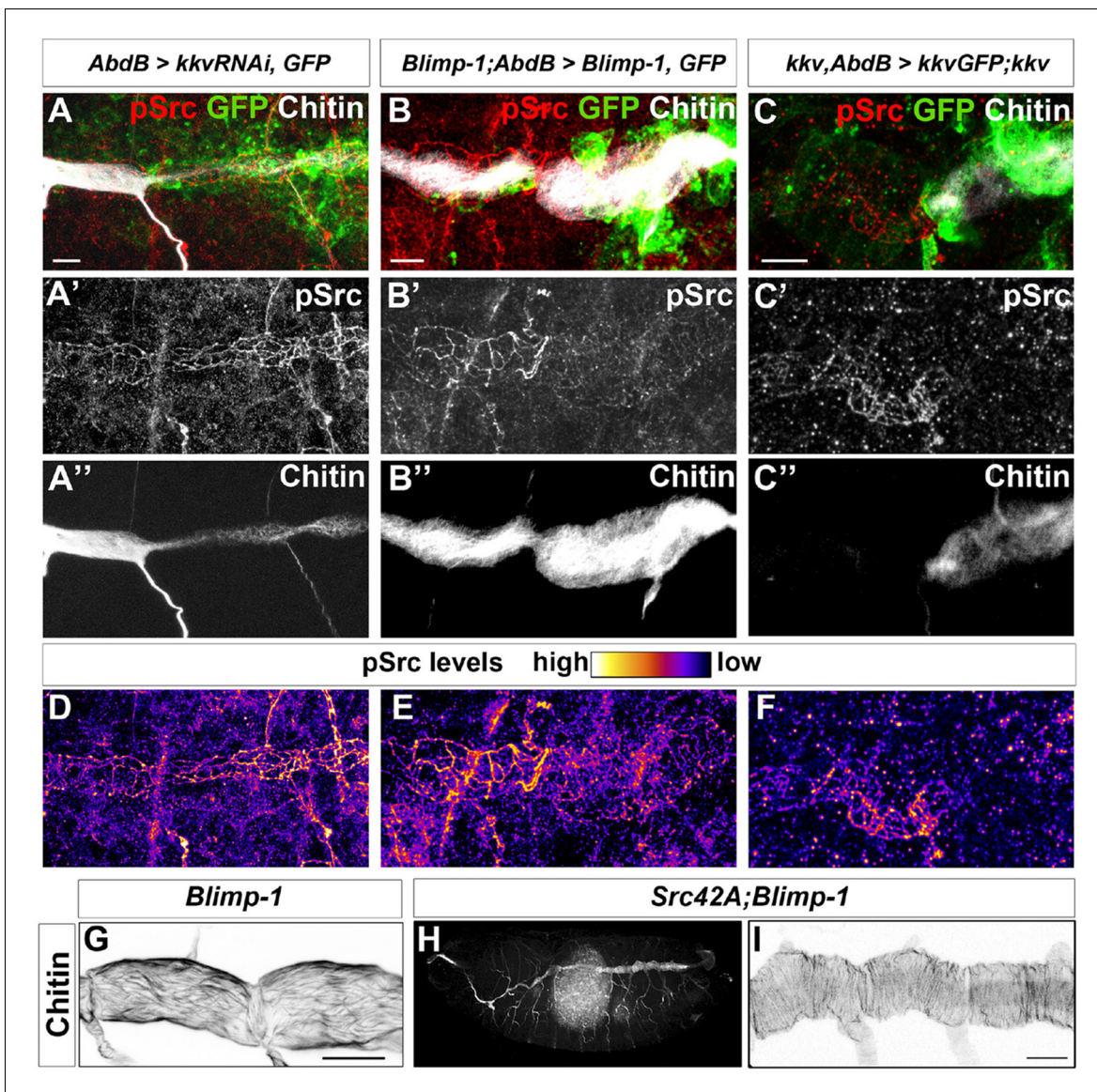


Figure 10. Chitin levels modulate Src activation. (A and D) Wild-type embryo expressing *AbdB-GAL4UASkkvRNAi* and *UASSrcGFP*, stained with anti-GFP (green, A) to visualise the *AbdB* domain, anti-pSrc (red, A') to detect activated Src42A, and fluostain (grey, A'') to label chitin. Levels of pSrc are better visualised in D, with a different colour-coded LUT. (B and E) *Blimp-1* mutant embryo, expressing *AbdB-GAL4UASBlimp-1* and *UASSrcGFP*, to rescue the *Blimp-1* phenotype at the posterior end of the embryo, stained with anti-GFP (green, B) to visualise the *AbdB* domain, anti-pSrc (red, B') to detect activated Src42A, and fluostain (grey, B'') to label chitin. Levels of pSrc are better appreciated in E, with a different colour-coded LUT. (C and F) *kkv* mutant embryo, expressing *AbdB-GAL4* and *UASkkvGFP*, to rescue the *kkv* phenotype at the posterior end of the embryo, stained with anti-GFP (green, C) to visualise the *AbdB* domain, anti-pSrc (red, C') to detect activated Src42A and fluostain (grey, C'') to label chitin. Levels of pSrc are better appreciated in F, with a different colour-coded LUT. Scale bars 10 μ m. (G-I) Late stage 16 embryos stained with fluostain to visualise taenidial organisation. (G) Detail of *Blimp-1* dorsal trunk showing taenidial disorganisation; (H) whole *Src42A;Blimp-1* double mutant, showing some of the characteristic *Blimp-1* tracheal phenotypes; (I) Detail of *Src42A;Blimp-1* double mutant dorsal trunk showing rescued taenidial organisation. Scale bars 25 μ m.

DOI: 10.7554/eLife.09373.019

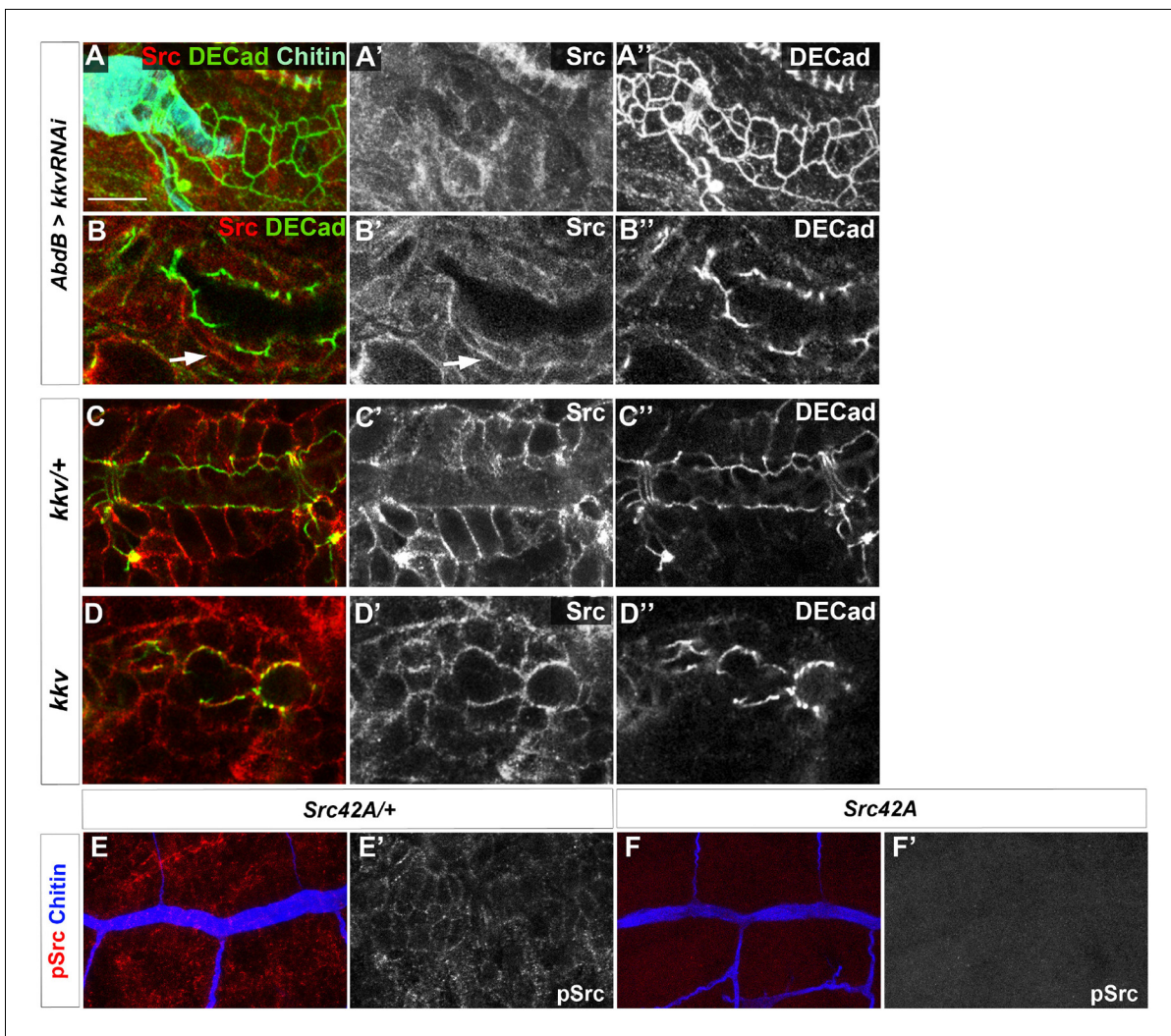


Figure 10—figure supplement 1. Src protein levels in *kkv* mutant trachea. (A, B) Wild-type embryo expressing *AbdB GAL4 UAS kkvRNAi* stained with anti-Src (red, A and A', B and B') to detect Src42A protein and anti-DE-Cad (green, A and A', B and B'). In panel A we also detected chitin with fluostain. (A) is a projection of confocal sections and (B) is a single section. (C) *kkv* heterozygous embryo stained with anti-Src (red, C and C') to detect Src42A protein and anti-DE-Cad (green, C and C'). Image is a single confocal section. (D) *kkv* homozygous embryos stained with anti-Src (red, D and D') to detect Src42A protein and anti-DE-Cad (green, D and D'). Image is a single confocal section. (E) *Src42A* heterozygous embryo stained with anti-pSrc (red, E and E') to detect phosphorylated Src42A protein and CBP (blue, E). Image in E is a projection of confocal sections and in E' is a single confocal section. (F) *Src42A* homozygous embryo stained with anti-pSrc (red, F and F') to detect phosphorylated Src42A protein and CBP (blue, F). Images in F and F' are projections of confocal sections.

DOI: [10.7554/eLife.09373.020](https://doi.org/10.7554/eLife.09373.020)

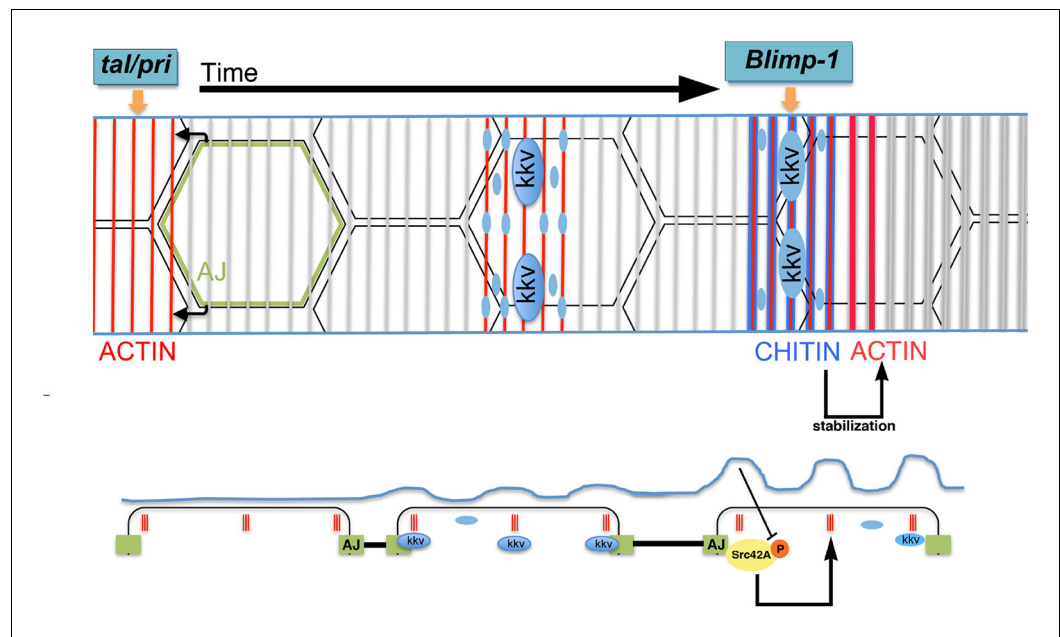


Figure 11. Proposed model for the generation of the supracellular taenidia. Model depicting the relationship between chitin synthesis and taenidial fold and F-actin organisation during taenidial fold formation. Drawn is the dorsal trunk at later stages of embryonic development and the effects of Tal/Pri, Blimp-1 and Kkv on F-actin and chitin organisation, respectively. This schematic representation depicts a time progression of events in taenidial formation. Large blue circles represent the Kkv localisation that is predominant within each taenidium, but it is also found in 'non-taenidial' regions of the membrane (smaller blue circles). The inhibitory effect of chitin in Src42A activation is depicted and well as the feedback from this inhibition back to the stabilisation of the F-actin rings. DOI: [10.7554/eLife.09373.021](https://doi.org/10.7554/eLife.09373.021)